Experimental Mechanics of Materials
Group 1

Thijs Rikkerink (3259293)
Rick Assink (3263657)
Oriol Jo López (3759431)

September-November 2025

Contents

1 Introduction

Understanding material behavior and using the material properties to your advantage is vital for all structural uses. Materials in the real world are subjected to a variety of load mechanisms, from axial loads to flexural loads and cyclic loads. The best way to investigate these mechanisms is to experimentally test the materials in a controlled environment in these mechanisms. This report focuses on experimentally determining material properties and behavior mechanisms, such as deformation and failure mechanisms, using tried and proved axial and flexural testing techniques. Testing a range of materials with diverging behavior using different methods to measure their displacement, including digital image correlation (DIC), finger extensometers, machine displacement, and strain gauges.

The objective of this report is to analyze the engineering and true stress-strain behavior of several materials under axial and flexural loads to compute their parameters. This report also investigates the accuracy and reliability of certain measurement techniques, determining relevant uncertainties and using these results to accurately describe the properties and behavior of the material.

2 Axial Testing

The following experiments are about axial testing; metal tensile tests with different metals and machine displacement, cyclic metal tensile tests with finger-extensometer, DIC and machine displacement, and polymer tensile tests with different polymers and different strain rates and machine displacement. The materials used for these tests are shown in table 1.

Table 1: Axial Testing Materials

Category	Type	Quantity
UTM	Zwick Roell Z005 [6]	1
UTM	Zwick Roell Z5.0 [8]	1
UTM	Zwick Roell Z100 Retro Line [6]	1
Calipers	Holex ABS [2]	2
Micrometer	Mitutoyo IP65 [3]	1
Specimen	Copper Dogbone	4
Specimen	Copper Dogbone with Speckle	1
Specimen	Aluminium Dogbone	2
Specimen	Cast PMMA Dogbone	9
Specimen	Extruded PMMA Dogbone	1
Specimen	PP Dogbone	1
Specimen	PS Dogbone	1

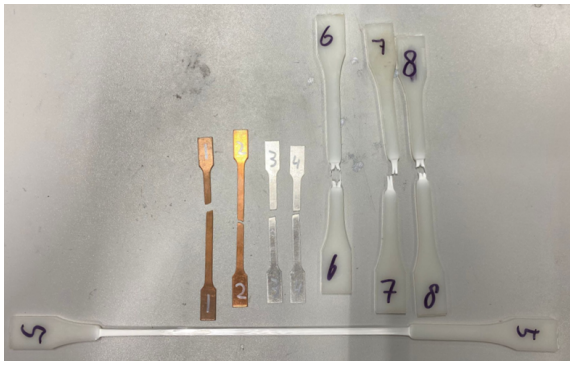

Figure 1: Experiment 1: Metallic Tensile Testing Specimens

2.1 Metallic Materials

For this section, 8 samples including 2 copper samples, 2 aluminum samples, and 4 polypropylene samples were tested until failure in a Universal Testing Machine (UTM). The machine compliance of this UTM was also tested to compensate for the additional displacement of the machine. Only the 4 metal samples with corrected machine compliance will be reported here, as a much more detailed polymer experiment was conducted since then, which will be reported in Section 2.3. These metal samples were tested on September 18th 2025 on the Zwick Roell Z005. The pulling speed was 30 mm/min, with a preload of 10 N. During the experiment the room conditions were as follows: Temperature [ºC]: 21, Humidity [%rH]: 69.2. The measurements taken of the specimens are shown in table 2, and a picture of the specimens is in figure 3.

Table 2: Experiment 1 specimen size measurements

Specimen	Width Measurement				Thickness Measurement			
⋮	1 [mm]	2 [mm]	3 [mm]	Mean [mm]	1 [mm]	2 [mm]	3 [mm]	Mean [mm]
Copper 1	5.05	5.05	5.06	5.05	0.990	0.995	0.992	0.992
Copper 2	5.02	5.01	5.04	5.02	0.994	0.996	0.988	0.993
Aluminium 3	5.09	5.02	5.03	5.05	0.996	0.988	1.013	0.999
Aluminium 4	5.08	5.06	5.08	5.07	1.001	0.999	1.002	1.001

2.1.1 Stress-Strain Curve & Parameter Comparison

In the stress-strain curves shown in figure 12 and the parameters in tables 3 and 4, multiple observations can be made. It is immediately clear that the two copper samples closely resemble each other's behavior, where the aluminum samples have a clear difference in their strength. This is the result of a user error, as specimen aluminum 3 was clamped slightly tilted, which made its cross-section perpendicular to the principal direction slightly larger, thus increasing it's strength and stiffness in this direction.
The work hardening properties of copper are also clearly visible, as the stress continues to increase far beyond the yield strength, while for aluminum, the tensile strength is only slightly above the yield strength. This goes for both the true and engineering parameters, although the true stresses are evidently higher because

of the decreasing cross-section.
Notably, the toughness of both the true and engineering curves is the same. This is because toughness is a physical phenomenon, describing the energy absorbed by the material during the test, therefore it is independent of stress-strain calculations. The resilience not being exactly the same is due to the elastic region being slightly larger for the true calculations, shown by its higher yield strength.

2.1.2 Engineering/True Stress Calculations

The engineering parameters make for simpler computation in linear-elastic analyses. They cannot be assumed to be accurate beyond these small deformations, as the cross-sectional change, which is not taken into account, starts having a large effect on the material behavior. The true parameters are nearly identical to the engineering parameters in this elastic region, but are far more accurate for describing material behavior during plastic deformation scenarios, as they take the changing cross-sectional area into account. This, however, complicates their computation, which is why engineering parameters should be used when they are sufficient.

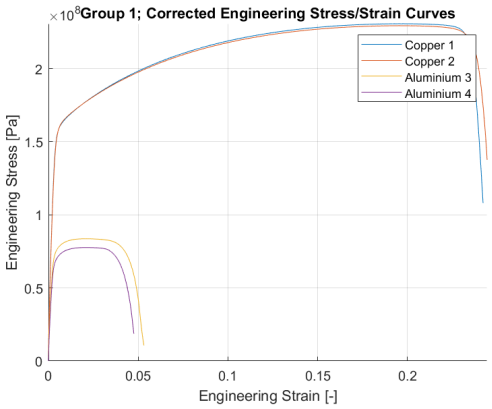

((a)) Engineering Stress-Strain Curve

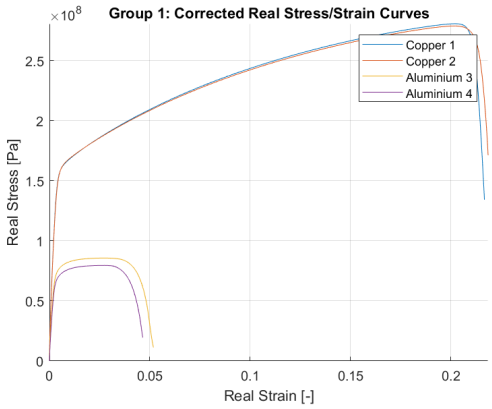

((b)) True Stress-Strain Curve

Figure 2: Experiment 1: Engineering and True Stress-Strain Curves

Table 3: Engineering properties of the samples from Experiment 1

Property	**Copper 1**	**Copper 2**	**Aluminum 3**	**Aluminum 4**
Strain at break [-]	0.25	0.25	0.06	0.05
Stress at break [MPa]	108.06	137.63	10.67	18.68
Ultimate stress [MPa]	230.74	229.41	83.67	77.65
Yield stress [MPa]	158.96	158.83	77.19	70.60
Young's modulus [GPa]	147.70	148.44	87.02	89.37
Resilience $[\frac{kJ}{m^3}]$	644.41	626.44	296.83	244.23
Toughness $[\frac{kJ}{m^3}]$	51121.16	51498.13	3912.16	3274.79

Table 4: True properties of the samples from Experiment 1

Property	Copper 1	Copper 2	Aluminum 3	Aluminum 4
Strain at break [-]	0.22	0.22	0.05	0.05
Stress at break [MPa]	134.23	171.26	11.24	19.57
Ultimate stress [MPa]	280.68	278.83	85.68	79.54
Yield stress [MPa]	160.91	160.70	78.06	71.45
Young's modulus [GPa]	151.39	152.09	88.74	91.27
Resilience $[\frac{kJ}{m^3}]$	697.62	669.70	318.47	263.59
Toughness $[\frac{kJ}{m^3}]$	51121.16	51498.13	3912.16	3274.79

2.1.3 Uncertainty Analysis

When conducting the experiment, multiple errors were introduced. The main perpetrators of these errors are the user, the equipment, and the environment. These errors are examined and quantified to account for them in the obtained results.

Uncertainty classification
To classify the uncertainties, it first has to noted what elements of the experiment precisely contribute to the uncertainty. Firstly there is the specimen, whose behavior is influenced by unknown variations, such as the processing and the exact alloy composition. Then there is the measuring equipment, such as the calipers and micrometers that were used to measure the specimen. Then there is the UTM itself. Where the machine compliance has been taken into account, the variations in the load cell and grip-to-grip distance are still relevant.

Table 5: Sources of Uncertainty

Influencing Factor	Error type	Distribution	Error value
1:Width measurement (Calipers: Holex ABS) [2]			
Repeated measurements	A	Gaussian	±0.02 mm
Resolution	B	Uniform	±0.01 mm
Measurement Deviation E MPE	B	Gaussian	±0.03 mm
2:Thickness Measurement (Micrometer: Mitutoyo IP65) [3]			
Repeated measurements	A	Gaussian	±0.006 mm
Resolution	B	Uniform	±0.0005 mm
Precision	B	Gaussian	±0.001 mm
3:Grip-to-grip distance (Zwick Roell Z005) [6]			
Repeatability	B	Uniform	±0.002 mm
Resolution	B	Uniform	$0.96 * 10^{-6}$ mm
4:Force Measuring (KAF-W Force Transducer) [1]			
Accuracy	B	Gaussian	0.05 %
Repeatability	B	Uniform	±2.5 N

Combined standard uncertainty
To find the standard uncertainty for type A error, where for each measurement and n = 3 measurements were conducted, the following formula's are used:

$$Variance: \ \hat{s}^2(x) = \frac{1}{n-1}\sum_{i=1}^{n}(x_i - \bar{x})^2 \quad Standard\,Uncertainty: \ u_{\bar{x}} = \frac{\hat{s}}{\sqrt{n}} \tag{1}$$

This gives the following standard uncertainty for the sample width and thickness:

Table 6: Type A Error: Standard Uncertainties

Specimen	Width $u_{\bar{x}}$ [mm]	Thickness $u_{\bar{x}}$ [mm]
Copper 1	± 0.0050	± 0.0015
Copper 2	± 0.0091	± 0.0024
Aluminum 3	± 0.0220	± 0.0074
Aluminum 4	± 0.0071	± 0.0009

To find the standard uncertainty for type B error, each separate uncertainty first has to be converted to a standard uncertainty using their distribution. For the two distributions seen in table 5, where b is the standard deviation, these are converted as:

$$Uniform\ Distribution:\ u(x) = \frac{b}{\sqrt{3}}\quad Gaussian\ Distribution:\ u(x) = b \tag{2}$$

This gives the following standard uncertainties for the type B errors:

Table 7: Type B Error: Standard Uncertainties

$u_{res,1}$ [mm]	$u_{dev,1}$ [mm]	$u_{res,2}$ [mm]	$u_{prc,2}$ [mm]	$u_{rep,3}$ [mm]	$u_{res,3}$ [mm]	$u_{rep,4}$ [N]	$u_{acc,4}$ [%]
± 0.0057	± 0.03	± 0.0003	± 0.001	± 0.0012	$\pm\ 0.55 * 10^{-6}$	± 1.4434	0.05

The Type A and Type B standard uncertainties are combined using the quadrature rule to create combined standard uncertainties. This is shown per parameter in table 8. Not that the engineering and true properties are not shown separate, as the uncertainty does not depend these methods and is therefore unchanged. This also applies to all stresses, as they have the same sources of uncertainty and thus the same errors.

Table 8: Combined standard uncertainties of the experiment 1 parameters

Property	**Copper 1**	**Copper 2**	**Aluminum 3**	**Aluminum 4**
Strain at break [-] $*10^{-5}$	±2.3322	±2.3314	±2.3324	±2.3314
Stress at break [MPa]	±0.2881	±0.2896	±0.2861	±0.2844
Ultimate stress [MPa]	±0.2881	±0.2896	±0.2861	±0.2844
Yield stress [MPa]	±0.2881	±0.2895	±.2861	±0.28441
Young's modulus [GPa]	±2.4522	±2.3687	±1.4209	±1.2477
Resilience $[\frac{kJ}{m^3}]$	±1.2086	±1.1744	±1.1338	±1.0162
Toughness $[\frac{kJ}{m^3}]$	±136.30	±108.35	±104.87	±49.864

2.2 Strain Measurement

In these experiments, 3 copper specimens were tested by axial cyclic loading. For all 3 specimens, a different measuring technique was used to determine the displacement; an extensometer, DIC, and machine displacement. All 3 specimens were measured 3 times to find the width and thickness, with this an average width and thickness were determined along with a corrected sample standard deviation. A picture of the specimens is in figure 3.

Table 9: Sample width measurements

Specimen	**w [mm]**	**w [mm]**	**w [mm]**	$\mathbf{w}_{avg}$ **[mm]**	**S [mm]**
Copper 1	5.05	5.06	5.08	5.06	±0.02
Copper 2	5.09	5.09	5.09	5.09	±0.00
Copper 3	5.05	5.04	5.05	5.05	±0.01

Table 10: Sample thickness measurements

Specimen	**t [mm]**	**t [mm]**	**t [mm]**	$\mathbf{t}_{avg}$ **[mm]**	**S [mm]**
Copper 1	1.003	1.005	0.996	1.001	±0.005
Copper 2	1.003	0.986	0.994	0.994	±0.009
Copper 3	0.990	0.999	0.994	0.994	±0.005

Figure 3: Experiment 2: Metallic Cyclic Tensile Testing Specimens

The specimen named Copper 1 had its displacement measured by a finger extensometer, Copper 2 with DIC, and Copper 3 with machine displacement, which was then compensated for machine compliance using the infinetly stiff specimen test from experiment 2.
The experiment was conducted on 25-09-2025. Copper 1 was testing on the Zwick Roell Z100 Retro Line [6], Copper 2 on the Zwick Roell Z005 [6], and Copper 3 on the Zwick Roell Z5.0 [8]. The pulling speed was 30 mm/min and the pre-load was 10 N. The ambient temperature and humidity were not measured, but are likely similar to those of section 2.1.
This cyclic test was not performed till failure of the material, which resulted in only the following properties to be determined: yield stress, Young's modulus, and resilience for both the engineering values and true values.

2.2.1 Extensometer

The first specimen was tested in the Zwick Roell Z100-Retro line, using screw clamps and an extensometer to measure displacement. This data resulted in a force-displacement curve, from which engineering and true stress-strain curves were determined.

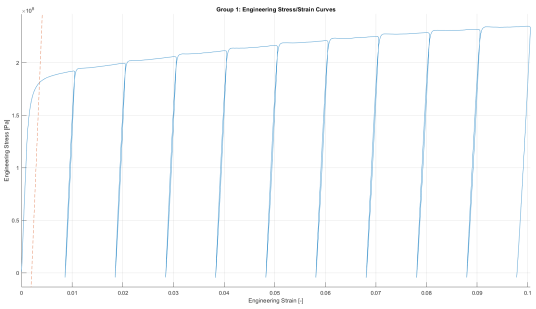

((a)) Engineering Stress-Strain Curve

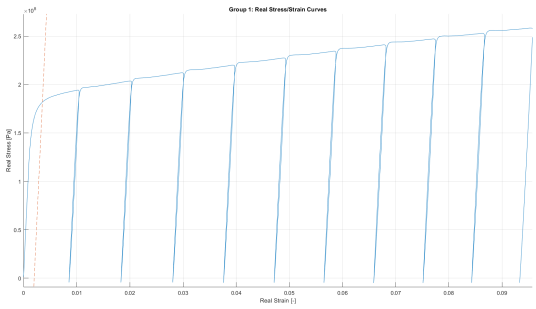

((b)) True Stress-Strain Curve

Figure 4: Experiment 2: Engineering and True Stress-Strain Curves using the extensometer

Using this data, the real and engineering material properties were determined. The Young's modulus was determined using the 0.002 strain offset line method as shown in figures 4(a) and 5(b)

Table 11: Engineering and true properties of the material using an extensometer

Property	**Engineering Value**	**True Value**
Yield stress [MPa]	181.36	182.00
Young's modulus [GPa]	117.87	118.02
Resilience $[\frac{kJ}{m^3}]$	485.07	485.07

The values for the yield stress and Young's modulus are close together for the engineering and real values, this results in a resilience which is nearly identical.

2.2.2 Digital image correlation (DIC)

The machine used for this experiment was the Zwick-Roell Z005 using wedge clamps and a DIC setup.

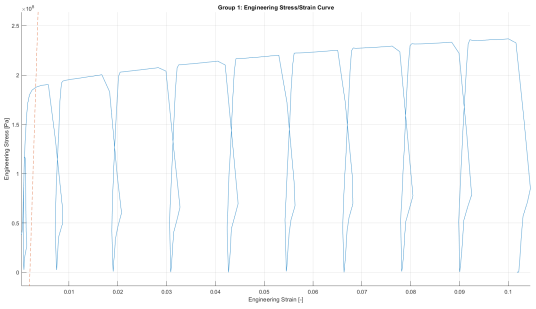

((a)) Engineering Stress-Strain Curve

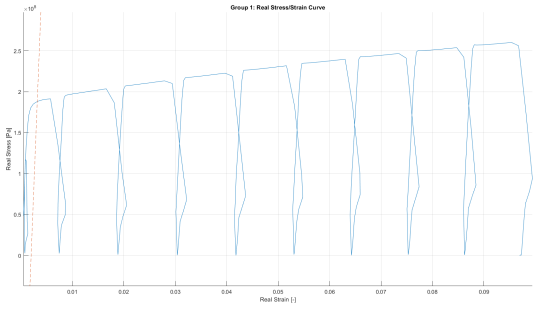

((b)) True Stress-Strain Curve

Figure 5: Experiment 2: Engineering and True Stress-Strain Curve using DIC

These curves show irregular behavior in the loading and unloading phase; this can be explained by the clamps, as this experiment is the only cyclic experiment using wedge clamps. while unloading the clamps are able to move a small amount this results in a change of displacement and strain.

Table 12: Engineering and true properties of the material using DIC

Property	Engineering Value	True Value
Yield stress [MPa]	187.77	188.39
Young's modulus [GPa]	157.47	157.81
Resilience $[\frac{kJ}{m^3}]$	511.02	511.02
Average Poisson's ratio [-]	0.4186	

Note that because there was a cycle in the elastic region, the Young's modulus and resilience could not be calculated as accurate as desired. Due to the irregular loading and unloading behavior, the Poisson's ratio might be less accurate as well.

2.2.3 Machine displacement

This experiment was performed on the specimen named Copper 3 using the Zwick-Roell Z5.0 with screw clamps, and the test was machine compliance corrected. This resulted in the stress-strain curves pictured in figure 6.

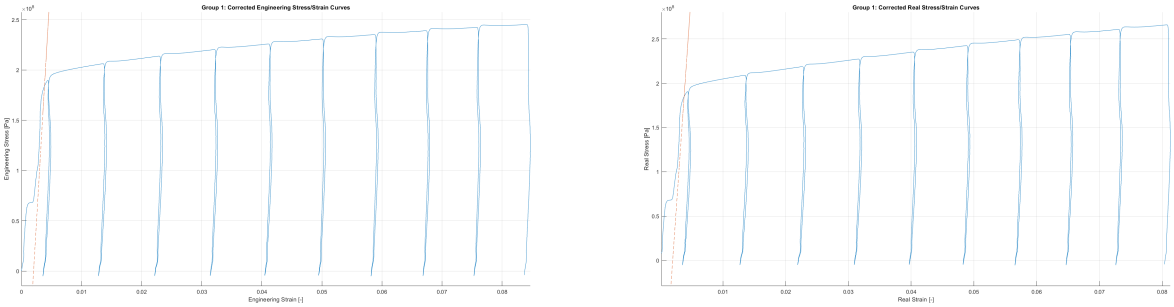

((a)) Engineering Stress-Strain Curve

((b)) True Stress-Strain Curve

Figure 6: Experiment 2: Engineering and True Stress-Strain Curves using machine displacement

This resulted in the material properties shown in table 13.

Table 13: Engineering and true properties of the material using machine displacement

Property	Engineering Value	Real Value
Yield stress [MPa]	183.14	183.83
Young's modulus [GPa]	106.35	106.49
Resilience $[\frac{kJ}{m^3}]$	326.76	326.76

2.2.4 Comparison of the Parameters for Different Strain Measurements

In table 14 the parameters are placed next to each other. The higher Young's modulus of the DIC is easily seen here, which is, as mentioned before, likely caused by the cycle in the linear-elastic part of the stress-strain curve. The variation in the resilience is probably caused by the machine displacement curve having a "hump" in its linear-elastic part. This is likely due to a mistake in the script for the machine compliance compensation, as this code was written for a non-cyclic test. the "S" value shows the corrected sample standard deviation calculated using equation 3. The combined standard uncertainties of all parameters can be found in table 16.

$$S = \sqrt{\frac{1}{N-1}\sum_{i=1}^{N}(x_i - \bar{x})^2} \tag{3}$$

Table 14: Engineering results comparison

Property	Extensometer	DIC	MD	mean	S
Yield stress [MPa]	181.36	187.77	183.14	184.09	±3.31
Young's modulus [GPa]	117.87	157.47	106.35	127.23	±26.24
Resilience $[\frac{kJ}{m^3}]$	485.07	511.02*	326.76*	440.95	±99.74

2.2.5 Uncertainty Analysis

To determine the uncertainty of the parameters in tables 11, 12 and 13, a budget of uncertainties must be made. This budget contains the uncertainties with a relatively large impact on the combined uncertainties, and is shown in table 15

Table 15: Sources of Uncertainty

Influencing Factor	Error type	Distribution	Error value
1:Width measurement (Calipers: Holex ABS) [2]			
Repeated measurements	A	Gaussian	±0.003 mm
Resolution	B	Uniform	±0.01 mm
Measurement Deviation E MPE	B	Gaussian	±0.03 mm
2:Thickness Measurement (Micrometer: Mitutoyo IP65) [3]			
Repeated measurements	A	Gaussian	±0.004 mm
Resolution	B	Uniform	±0.0005 mm
Precision	B	Gaussian	±0.001 mm
3:Copper 1 Extensometer Tool Separation (Zwick Roell Z100 Retro Line) [7]			
Repeatability	B	Uniform	±0.002 mm
3:Copper 2 DIC Measured Average Strain (Zwick Roell Z005)			
Frame rate	B	Uniform	2 fps
3:Copper 3 Grip-to-grip distance (Zwick Roell Z5.0) [8]			
Repeatability	B	Uniform	±0.002 mm
Resolution	B	Uniform	$0.17 * 10^{-4}$ mm
4:Copper 1 Force Measuring (Xforce K Force Cell) [5]			
Accuracy	B	Gaussian	0.2 %
Repeatability	B	Uniform	±20 N
4:Copper 2 Force Measuring (KAF-W Force Transducer) [1]			
Accuracy	B	Gaussian	0.05 %
Repeatability	B	Uniform	±2.5 N
4:Copper 3 Force Measuring (Xforce HP Force Cell) [5]			
Accuracy	B	Gaussian	0.2 %
Repeatability	B	Uniform	±5 N

Not all uncertainties in the budget are used for all experiments, for these non-universal uncertainties the specimen name where they are used is written next to them.
The type A and type B uncertainties from table 15 are then combined into combined standard uncertainties, per parameter and per experiment. This derivation is done similar to the one in section 2.1, so it will not be reported in detail. The resulting combined standard uncertainties are shown in table 16.

Table 16: Combined standard uncertainties of the experiment 2 parameters

Property	Copper 1	Copper 2	Copper 3
Yield stress [MPa]	±0.2797	±0.2853	±0.5751
Young's modulus [GPa]	±15.8182	±0.2376	±18.5540
Resilience $[\frac{kJ}{m^3}]$	±6.1416	±0.7760	±1.0237

In table 16 it is evident that the DIC data has fever uncertainties than the other strain measurement techniques. This can be explained by the lack of resolution or repeatability for the strain data, as well as that the DIC outputs strain instead of displacement, which then gains extra uncertainty from its derivation. This is especially visible in the Young's modulus.

2.2.6 General Comparison

To validate these results they were compared to other groups doing the same experiments. For group 2 the Poisson's ratio was not available. Table 17 shows the engineering values for the Young's modulus, yield stress, resilience, and the Poisson's ratio.

Table 17: Groups 2, 3 and 4 results

Group	**Method**	**Yield stress [MPa]**	**Young's modulus [GPa]**	**Resilience [$\frac{kJ}{m^3}$]**	**Poisson's ratio**
Group 2	Extenso	196.78	222.30	451.05	N/A
	DIC	193.11	93.75	491	N/A
	MD	190.79	26.13	615	N/A
Group 3	Extenso	129	130.19	77.4	N/A
	DIC	133	115.31	76.9	0.425
	MD	125	123.59	126	N/A
Group 4	Extenso	181.06	115.66	472.06	N/A
	DIC	189.7	87.861	423.99	0.3873
	MD	189.69	91.603	560.02	N/A

Comparing these results to those in table 14, it can be concluded that the results for the Young's modulus are closer to those of group 3, with the results of group 4 being lower. The results for the yield stress are very comparable to group 4, the results of group 3 seem relatively far off for the yield stress and resilience. This might be because of an error while calculating the yield stress, as the results of group 2 and 4 of the yield stress very similar. The results for the resilience are quite spread for all groups, where those of group 4 are the nearest to table 14. This spread likely has to do with the different methods of compensating the machine compliance for the machine displacement, which has the most effect on the linear-elastic zone and thus the resilience. As for the Poisson's ratio, the value from group 3 is closest to that of table 12.

2.3 Polymeric Materials

The polymeric materials were tested in two different variables. The first variable is the material, where four standard tensile tests were conducted on a universal testing machine, the Zwick Roell Z005. Each tensile test had a different material, as shown in table 19. The tests were conducted with a temperature of 25.3 ºC and a relative humidity of 41.1 %rH. The specimens had their width and thickness measured in three different locations, the values of which are noted in table 18 and their errors are noted in table 25. The pulling speeds are shown in tables 22 and 19, and a picture of the specimens after the test is shown in figure 7.

Figure 7: Experiment 3: Polymer Tensile Testing Specimens

Table 18: Experiment 3 specimen size measurements

Specimen	**Width Measurement**				**Thickness Measurement**			
⋮	**1 [mm]**	**2 [mm]**	**h3 [mm]**	**Mean**	**1 [mm]**	**2 [mm]**	**3 [mm]**	**Mean**
PS1	9.70	9.73	9.68	9.70	4.010	4.012	4.003	4.008
PP2	9.62	9.57	9.57	9.59	3.989	3.991	3.993	3.991
PMMA3e	9.67	9.72	9.71	9.7	3.839	3.836	3.836	3.837
PMMA4c	9.70	9.68	9.70	9.69	3.364	3.357	3.349	3.357
PMMA5c	9.76	9.77	9.77	9.77	3.366	3.356	3.351	3.358
PMMA6c	9.69	9.69	9.69	9.69	3.364	3.348	3.336	3.349
PMMA7c	9.73	9.75	9.76	9.75	3.468	3.493	3.580	3.514
PMMA8c	9.65	9.66	9.67	9.66	3.377	3.382	3.399	3.386
PMMA9c	9.72	9.71	9.73	9.72	3.590	3.552	3.483	3.542
PMMA10c	9.68	9.67	9.66	9.67	3.589	3.540	3.480	3.536
PMMA11c	9.70	9.68	9.69	9.69	3.406	3.390	3.381	3.392
PMMA12c	9.70	9.71	9.72	9.71	3.570	3.530	3.479	3.526

The force-displacement data was processed into stress-strain curves, which are in figures 8 and 10. From these curves both the engineering and true parameters are derived, which are then displayed in tables 20, 21, 23 and 24.

Table 19: Experiment 3 part 1 Specimen Information

Specimen	Material	$\dot{\epsilon}$ [mm/min]
PS1	Polystyrene	100
PP2	Polypropylene	100
PMMA3e*	Polymethyl Methacrylate Extruded	100
PMMA4c**	Polymethyl Methacrylate Cast	100

** The **raw material** from which the coupon was cut, is **extruded**. Not the specimen itself.*
*** The **raw material** from which the coupon was cut, is **cast**. Not the specimen itself.*

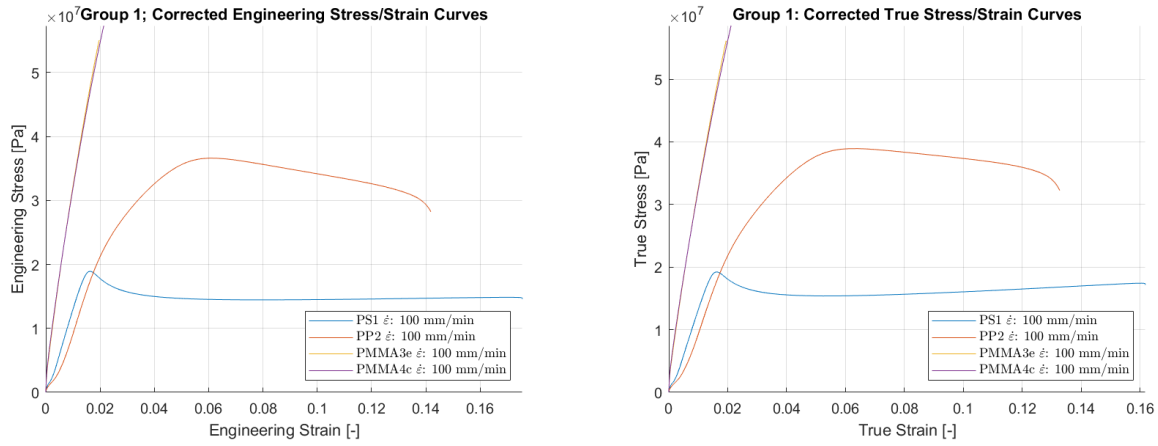

((a)) Engineering Stress-Strain Curve

((b)) True Stress-Strain Curve

Figure 8: Experiment 3, Different Polymers: Engineering and True Stress-Strain Curves

In the second part of experiment 3, cast polymethyl methacrylate (PMMAc) was tested at different strain rates as shown in table 22.

Table 20: Engineering material properties

Specimen	**E [GPa]**	σ_{yield} **[MPa]**	σ_{break} **[MPa]**	ϵ_{break} **[-]**	σ_{ult} **[MPa]**	U_r $[\frac{kJ}{m^3}]$	U_T $[\frac{kJ}{m^3}]$
PS1	1.3691	18.869	14.601	0.1756	18.912	157.01	2536.1
PP2	1.1445	3.2019	28.226	0.1419	38.918	8.1912	4227.2
PMMA3e	2.7840	-	54.910	0.0198	-	-	610.12
PMMA4c	2.6979	-	57.327	0.0214	-	-	692.55

Table 21: True material properties

Specimen	**E [GPa]**	σ_{yield} **[MPa]**	σ_{break} **[MPa]**	ϵ_{break} **[-]**	σ_{ult} **[MPa]**	U_r $[\frac{kJ}{m^3}]$	U_T $[\frac{kJ}{m^3}]$
PS1	1.3984	19.194	17.165	0.1618	19.221	159.53	2536.1
PP2	1.1738	3.1295	32.230	0.1327	38.918	7.8567	4227.2
PMMA3e	2.8527	-	55.997	0.0196	-	-	610.12
PMMA4c	2.7653	-	58.552	0.0211	-	-	692.55

Table 22: Experiment 3 part 2 Specimen Information

Specimen	$\dot{\epsilon}$ [mm/min]
PMMA5c	0.5
PMMA6c	1.6
PMMA7c	5
PMMA8c	16
PMMA9c	50
PMMA10c	160
PMMA11c	500
PMMA12c	1600

Using the results of this test the material properties could be determined. As this experiment was performed on a brittle material only 3 material properties were defined: the Young's modulus, the stress at break, and the strain at break.

Table 23: Engineering material properties

Specimen	**Young's modulus [GPa]**	**Stress at break [MPa]**	**Strain at break [-]**
PMMA5c	2.1863	48.540	0.0253
PMMA6c	2.3105	52.472	0.0267
PMMA7c	2.3828	52.481	0.0234
PMMA8c	2.4816	58.335	0.0265
PMMA9c	2.5761	41.473	0.0150
PMMA10c	2.7588	46.311	0.0165
PMMA11c	2.9157	56.814	0.0194
PMMA12c	2.9577	46.318	0.0170

Table 24: True material properties

Specimen	Young's modulus [GPa]	Stress at break [MPa]	Strain at break [-]
PMMA5c	2.2409	49.768	0.0250
PMMA6c	2.3675	53.871	0.0263
PMMA7c	2.4425	53.708	0.0231
PMMA8c	2.5429	59.878	0.0261
PMMA9c	2.6400	42.094	0.0149
PMMA10c	2.8304	47.078	0.0164
PMMA11c	2.9891	57.919	0.0192
PMMA12c	3.0305	47.105	0.0169

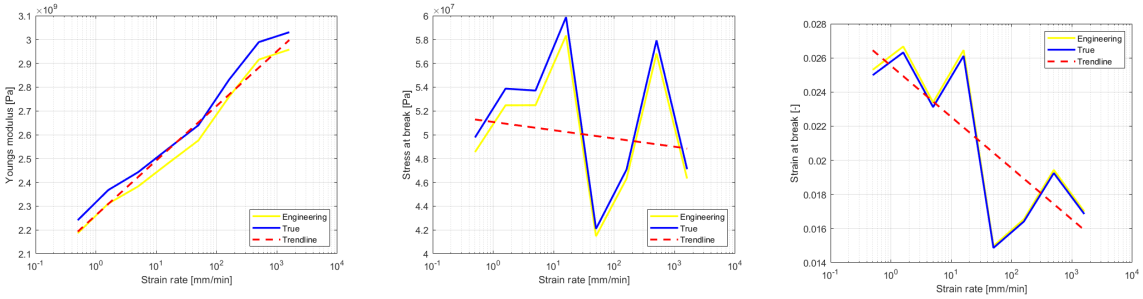

((a)) Young's modulus ((b)) Stress at break ((c)) Strain at break

Figure 9: Properties as a function of strain rate

2.3.1 Result Explanation

The brittle behavior can also be observed in the stress-strain curves in figure 10. Although the specimen with lower strain rates were not entirely linear elastic, it is still clear that the ultimate stress is nearly identical to the stress at break, and that there is no yield point or plastic deformation. The specimen with higher strain rates especially show this, where there is not even a small drop in strength before breaking. This is as expected, as the high strain rate does not allow for much viscous flow, therefore not allowing much deformation. In the lower strain rate samples, some more deformation and therefore a smaller stiffness is observed. This is also shown in figure 9(a). Interestingly, the ultimate strength is not directly linked to the strain rate. As seen in figure 9(b), there is a large deviation in the ultimate stress, where the trend line shows a decreasing stress for an increasing strain rate. As this does not follow literature [4], it must be caused by external differences. One of these is imperfections in the coupon. These were laser cut from a large cast sheet of PMMA, and due to the metal grid underneath the plate, some indentations were created when combined with the heat of the laser. This likely allowed the stress to propagate a crack from one of these indentations, making the specimen fail earlier.

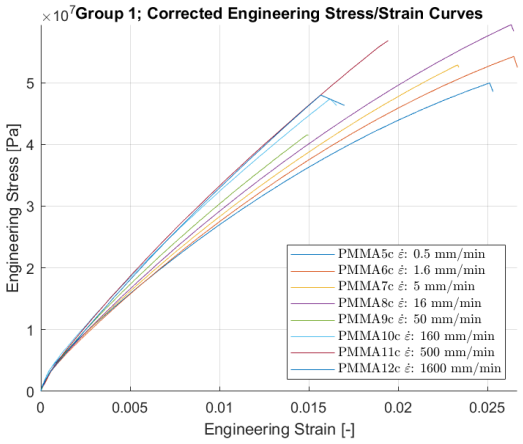

((a)) Engineering Stress-Strain Curve

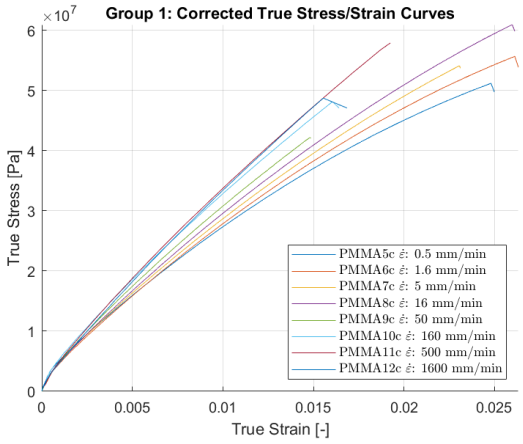

((b)) True Stress-Strain Curve

Figure 10: Experiment 3, Different Strain rates: Engineering and True Stress-Strain Curves

2.3.2 Uncertainty Analysis

To determine the uncertainty of the parameters of experiment 3, a budget of uncertainties is required. Since this experiment uses the same machine and tools as experiment 1, the uncertainty budget of experiment 3 is also shown in table 5.
The only difference are the repeated measurements, which have the error values shown in table 25.

Table 25: Repeated Measurement Average Uncertainties of Experiment 3

Influencing Factor	Error type	Distribution	Error Value
Repeated Width Measurements	A	Gaussian	± 0.012 mm
Repeated Thickness Measurements	A	Gaussian	± 0.013 mm

From the type A and B uncertainties, the combined standard uncertainties were determined for specimens 1 to 12. The derivation was done in detail in section 2.1 and will therefore not be reported fully here. The resulting combined standard uncertainties for the experiment 3 material parameters are shown in tables 26 and 27.

Table 26: Combined standard uncertainties of experiment 3 material variable parameters

Property	PS1	PP2	PMMA3e	PMMA4c
Strain at break [-] $*10^{-5}$	±1.4845	...	...	...
Stress at break [MPa]	±0.0371	±0.0377	±0.0388	±0.0444
Ultimate stress [MPa]	±0.0371	±0.0377	-	-
Yield stress [MPa]	±0.0371	±0.0377	-	-
Young's modulus [GPa]	±0.1396	±0.1195	±0.1902	±0.1578
Resilience $[\frac{kJ}{m^3}]$	±0.3092	±0.0965	-	-
Toughness $[\frac{kJ}{m^3}]$	±6.4521	±5.6652	±0.6286	±0.7203

Table 27: Combined standard uncertainties of experiment 3 strain rate variable parameters

Specimen	**Young's modulus [GPa]**	**Stress at break [MPa]**	**Strain at break [-]** $*10^{-5}$
PMMA5c	±1.0378	±0.0440	±1.4845
PMMA6c	±0.3205	±0.0445	⋮
PMMA7c	±0.4297	±0.0421	⋮
PMMA8c	±0.1958	±0.0412	⋮
PMMA9c	±0.1684	±0.0419	⋮
PMMA10c	±0.1386	±0.0270	⋮
PMMA11c	±0.0541	±0.0439	⋮
PMMA12c	±0.0189	±0.0422	⋮

Interestingly, the strain at break is the same for all specimens. There could still be differences that are smaller than what the rounded value allows for, but this trend shown that either the uncertainty of the strain at break is independent of the actual value, or more likely, that the code for this uncertainty is flawed. The value itself is, however, not unreasonable. Therefore it is probably not far from correct.

3 Flexural Testing

The following experiments are about flexural testing; polymer bending with machine displacement and using a strain gauge respectively. The materials used during these bending experiments are shown in table 28.

Table 28: Flexural Testing Materials

Category	Type	Quantity
UTM	Zwick Roell Z005 [6]	1
Calipers	Holex ABS [2]	2
Micrometer	Mitutoyo IP65 [3]	1
Specimen	Cast PMMA Coupon	3
Specimen	Extruded PMMA Coupon	2
Specimen	PP Coupon	2
Specimen	PS Coupon	2

3.1 Polymer Bending with Machine Displacement

The flexural tests performed in experiment 1 consisted of eight separate bending tests, four three-point bending tests and four four-point bending tests. These tests were performed in the Zwick Roell Z005, in a room with a temperature of 25.3°C and a room humidity of 59.8%.
The displacement data was compensated in post processing with the infinitely stiff specimen displacement data from experiment 2, same as with all previous machine displacement experiments.
The span of the bending setup was 71.65 mm, and for the 4-point bending jig the distance between the inner and outer support was 16.5 mm. The mid-plane was 38.8 mm.
The test was conducted with a pre-load of 5 N and the force was not tared as it was nearly equal to 0 already. The specimens were centered on the bottom supports by eye, as they had enough excess length to not slip off the supports during the test.
The width of the specimens was measured using digital calipers on three separate area, and the thickness was done similarly, except with a micrometer. The uncertainties caused by these measurements are taken into account in the uncertainty analysis. The width and thickness measurements are shown in table 29.
Some specimens also had visible imperfections, PMMA1c, PMMA2e and PMMA5c had little indentations, and PP3, PS4 and PP 7 had burrs. These were caused during their manufacturing, which was done by laser cutting the coupons from a sheet. PMMA6e and PS8 did not have any major visible imperfections. Since these imperfections were all on just one side of the specimens, this side was always oriented upwards during the test.
The PMMA specimens all had a brittle fracture during the test, where it was clear that the fracture started from the nearest visible imperfection. The PP and PS specimens did not fracture, but did experience some plastic deformation. During the test, these PP and PS specimens would eventually collide with the bottom or top of the bending fixture, which makes the measured values unusable, as it caused a spike in the force. These data points were removed in post processing. A photo of the specimens after the test is shown in figure 11

Figure 11: Experiment 4: 3-Point & 4-Point Bending Specimens

Table 29: Experiment 4 specimen size measurements

Specimen	**Width Measurement**				**Thickness Measurement**			
⋮	**1 [mm]**	**2 [mm]**	**3 [mm]**	**Mean [mm]**	**1 [mm]**	**2 [mm]**	**3 [mm]**	**Mean [mm]**
PMMA 1c	19.68	19.66	19.66	19.67	3.452	3.469	3.441	3.454
PMMA 2e	19.73	19.78	19.74	19.75	3.843	3.842	3.849	3.845
PP 3	19.82	19.78	19.80	19.80	3.993	4.002	4.001	3.999
PS 4	19.62	19.59	19.58	19.60	4.019	4.016	4.012	4.016
PMMA 5c	19.69	19.71	19.74	19.71	3.348	3.350	3.357	3.352
PMMA 6e	19.67	19.70	19.71	19.69	3.863	3.853	3.850	3.855
PP 7	19.57	19.54	19.54	19.55	4.006	4.015	4.020	4.014
PS 8	19.61	19.66	19.60	19.62	3.990	3.992	3.995	3.992

3.1.1 Result Derivation

The force-displacement data must be converted to normalized stress-strain data to calculate the material parameters. The bending tests might give slightly different parameters than the tensile tests, mostly due to assumptions made in the processing of the results, such as Euler's beam theory, which assumes that the cross-sectional areas of a beam remain perpendicular to it's neutral axis and therefore ignores the shear and rotational inertia of these cross-sections. Especially in large deformations this could have an effect, which means it likely plays a larger role in the more ductile PP and PS samples.
To process the force-displacement data into stress-strain data, a different approach than that of the tensile tests should be used. The utilized formulas of the flexural stress, flexural strain and flexural modulus of both the 3-point and 4-point bending is shown in equations 4 and 5, with their parameters displayed in table 30.

$$\sigma_f = \frac{3FL}{2bd^2} \quad \epsilon_f = \frac{6\delta_{max}d}{L^2} \tag{4}$$

Since δ_{max} is not the same as δ_{tool} for 4-point bending, we also need to derive δ_{max} as a function of δ_{tool} and other known parameters.

$$\sigma_f = \frac{3F(L-2a)}{2bd^2} \quad \epsilon_f = \frac{6\delta_{max}d}{L^2} \quad \delta_{max} = \frac{\delta_{tool}(3L^2-4a^2)}{12aL-16a^2} \tag{5}$$

Table 30: Flexural Testing Units

Parameter	Span	Width	Thickness	Load-Support Roller Distance	Force	Displacement
Unit	L	b	d	a	F	δ

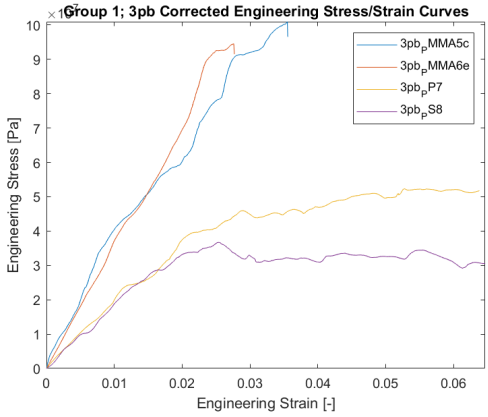

((a)) 3-Point Bending Stress-Strain Curve

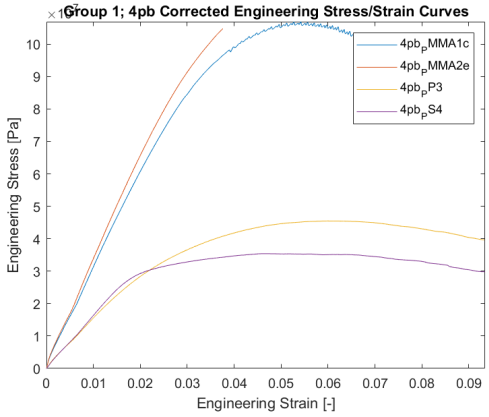

((b)) 4-Point Bending Stress-Strain Curve

Figure 12: Experiment 4: 3 & 4-Point Bending Stress-Strain Curves

Table 31: Material properties 4-point bending

Specimen	**Flexural modulus [GPa]**	$\sigma_{yield,flex}$ **[MPa]**	σ_{break} **[MPa]**	ϵ_{break} **[-]**	U_r $[\frac{kJ}{m^3}]$
PMMA1c	3.0240	-	101.10	0.0665	5054.3.6
PMMA2e	3.2729	-	104.79	0.0376	2213.9
PP3	1.4773	31.605	-	-	405.97
PS4	1.6167	29.403	-	-	325.56

Table 32: Material properties 3-point bending

Specimen	**Flexural modulus [GPa]**	$\sigma_{yield,flex}$ **[MPa]**	σ_{break} **[MPa]**	ϵ_{break} **[-]**	U_r $[\frac{kJ}{m^3}]$
PMMA5c	3.4398	-	96.588	0.0356	2039.6
PMMA6e	3.4879	-	91.504	0.0277	1365.2
PP7	1.8148	40.432	-	-	545.87
PS8	1.8178	33.555	-	-	372.53

3.1.2 Result Explanation

The first thing that stands out in the stress strain curves is that the curves in the 4-point bending test (figure 12(b)) are relatively smooth compared to the 3-point bending test (figure 12(a)), the most likely reason for this is a form of slip behavior as in the 3-point bending test there is only 1 contact point from the top, providing less stability then the 2 points of contact from above in the 4-point bending test. A clear distinction between the brittle behavior in PMMA2e, 4c, and 6e and the ductile behavior of the PP and PS can be seen, PMMA1c however shows ductile behavior with clear yielding. In the material properties are interesting results as well, comparing the results from the 4-point bending test in table 31: The flexural modulus and the flexural yield stress are higher in the 3-point bending test (table 32) while the stress and strain at break are both lower than in the 4-point bending test. Because the 3-point bending test has only one contact point at the top it creates a higher stress concentration, while possibly creating small indentation on the specimen at the point of maximum bending moment, causing failure at lower stress and strain.

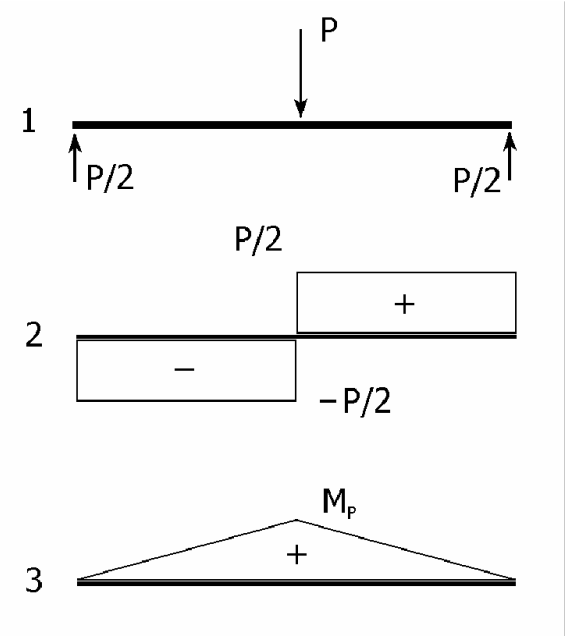

((a)) 3-Point Bending FBD, moment and shear diagrams

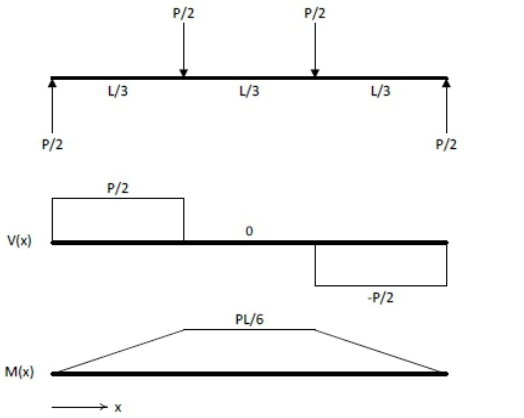

Figure 2 Free-body, shear force, and bending moment diagrams for a simply supported beam in four-point bending mode

((b)) 4-Point Bending FBD, moment, and shear diagrams

Figure 13: Experiment 4: 3 & 4-Point Bending FBD, moment, and shear diagrams

3.1.3 Elasticity Modulus Comparison

Now that there are data on polymer 3-point bending, 4-point bending, and tensile engineering elasticity, they can be displayed side by side, as shown in table 33. The PMMAc Young's modulus is taken from the PMMA4c specimen.

Table 33: Polymer Engineering Elasticity Modulus Comparison

Material	3pb Flexural [GPa]	4pb Flexural [GPa]	Young's [GPa]
PP	1.8148	1.4773	1.1445
PS	1.8178	1.6167	1.3691
PMMAe	3.4879	3.2729	2.7840
PMMAc	3.4398	3.0240	2.6979

The flexural modulus is highest for 3pb, then 4pb and then tensile. the difference between 3pb and 4pb is likely caused by the spiky 3pb data, as seen in figure 12(a). The 4pb being less spiky probably has to do with the constant bending moment between the load points, as seen in figure 13(b). The Young's modulus being slightly lower is to be expected, as the flexural modulus consists of both tensile and compressive stiffness, where the Young's modulus in this case is purely tensile. This compressive stiffness is often higher in polymer than their tensile stiffness, as the chains are not only stretched, but also pushed together. The latter action can be resisted by dipole intermolecular interactions, making it harder to compress the polymer. This is, however, only the case for PMMA, as PP and PS are not dipole. The increase in PP and PS stiffness is due to polymer chains being less prone to breaking when they are pushed closer together rather than pulled apart [10]. Another factor which may cause the difference between the flexural and Young's moduli, is the strain rate. The strain rate of the bending tests was 10 mm/min, where the tensile test was conducted at 100 mm/min. The higher strain rate allows for less viscous flow on a micro level in the polymers, making them less elastic.

3.1.4 Uncertainty analysis

To determine the uncertainty of the parameters of experiment 4, a budget of uncertainties is required. This test did not use the same clamping set up as experiment 1, but did use the same machine and tools. Considering that the clamp setup is accounted for in post-processing and is therefore not added to the uncertainty budget of experiment 1, the uncertainty budget of experiment 4 can be concluded to be the same as the one in table 5.
However, the only differences are again the repeated measurements, which have the error values shown in table 34.

Table 34: Repeated Measurement Average Uncertainties of Experiment 4

Influencing Factor	**Error type**	**Distribution**	**Error Value**
Repeated Width Measurements	A	Gaussian	± 0.013 mm
Repeated Thickness Measurements	A	Gaussian	± 0.003 mm

From the type A and B uncertainties, the combined standard uncertainties were determined for specimens 1 to 8. Since the derivation was already done in detail in section 2.1, it not be detailed here. The derived combined standard uncertainties for the experiment 4 material parameters are shown in tables 35 and 36.

Table 35: Combined standard uncertainties experiment 4: 4-point bending

Specimen	**Flexural modulus [GPa]**	$\sigma_{yield,flex}$ **[MPa]**	σ_{break} **[MPa]**	ϵ_{break} **[-]** $*10^{-4}$	U_r $[\frac{kJ}{m^3}]$
PMMA1c	±0.3504	-	±0.0212	±5.1889	±39.4293
PMMA2e	±0.4213	-	±0.0190	±4.2723	±25.1703
PP3	±0.2126	±0.0182	-	-	±31.7450
PS4	±0.2831	±0.0183	-	-	±37.0648

Table 36: Combined standard uncertainties experiment 4: 3-point bending

Specimen	**Flexural modulus [GPa]**	$\sigma_{yield,flex}$ **[MPa]**	σ_{break} **[MPa]**	ϵ_{break} **[-]** $*10^{-4}$	U_r $[\frac{kJ}{m^3}]$
PMMA5c	±0.3986	-	±0.0218	±5.1889	±29.7639
PMMA6e	±0.4490	-	±0.0190	±1.9016	±21.0599
PP7	±0.2612	±0.0183	-	-	±7.9687
PS8	±0.3183	±0.0184	-	-	±35.7497

The strain at break for PMMA1c and PMMA5c is the same rounded value, which makes sense considering that they are the same material, just in a different type of test. In general, most uncertainties lie quite close to each other.

3.2 Polymer Bending with a Strain Gauge

For experiment 2 another 3 bending tests were performed, consisting of one 3-point bending test and two 4-point bending tests. For all tests the same specimen was used. Strain was measured using a strain gauge, and for the 4-point bending test the strain was measured with the strain gauge on the top and in the second 4-point bending test with the strain gauge on the bottom of the specimen. In the 3-point bending test only the test with the strain gauge on the bottom was performed, because if the strain gauge would be on the top the contact point would be on the strain gauge itself. This specimen was only tested in the linear elastic region to not have plastic deformation, making this specimen reusable. Because of this the only material property that could be determined is the flexural modulus.
The tests were conducted on a Zwick Roell Z005 [6], with a room temperature of 21.3°C and a room humidity of 57.3 %. The specimen size measurements can be found in table 37.

Table 37: Experiment 5 specimen size measurements

Specimen	**Width Measurement**				**Thickness Measurement**			
⋮	**1 [mm]**	**2 [mm]**	**3 [mm]**	**Mean [mm]**	**1 [mm]**	**2 [mm]**	**3 [mm]**	**Mean [mm]**
PMMA 1e	19.71	19.70	19.69	19.70	3.849	3.847	3.849	3.848

3.2.1 Result Derivation

To derive the Young's moduli from the strain measured by the strain gauge and the force measured by the force cell, it first has to be determined what is being measured. The strain gauge measures, depending on the experiment, the bottom or top of the specimen. This means that it is only measuring the strain on the surface, which is either tensile or compressive. As shown in figure 14, the stress and strain on the surface are the maximum stress and strain of the specimen. It can therefore be concluded that the strain measured by the strain gauge is either the maximum compressive or tensile strain in the specimen, and that the Young's modulus on the surface can be found by dividing it by the maximum stress. Formulas for these calculations are shown in equation 6, where the parameters are described in table 30.

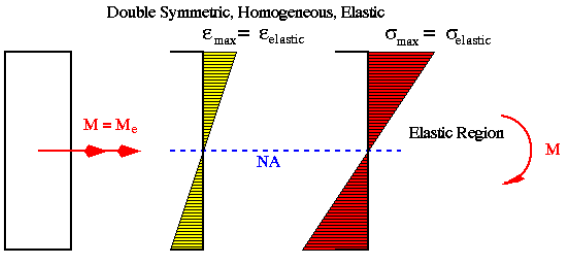

Figure 14: Stress-Strain distribution in elastic deformation [9]

$$\sigma_{max,3pb} = \frac{3FL}{2bd^2} \quad \sigma_{max,4pb} = \frac{3F(L-2a)}{2bd^2} \quad E_{3pb} = \frac{\sigma_{max,3pb}}{\epsilon_{3pb\ surface}} \quad E_{4pb} = \frac{\sigma_{max,4pb}}{\epsilon_{4pb\ surface}} \tag{6}$$

The max stresses were first calculated from the raw force data from the UTM, and the strain gauge data was cleaned up in post processing, by removing all data points from after the maximum force, and all data points before the strain started to change. The first strain data point was then used as a reference, removing it from all other strain points. This gave strain values which started at 0, and went to the maximum strain of the test. The tests for the 4pb specimen were done until 1.5 mm for deformation on the load points, which is not the same as the maximum deformation. The actual maximum deformation is calculated using third formula in equation 5, and is equal to 2.18 mm. The 3pb specimen was deformed to 2 mm, which is the maximum deformation as its load point lies in the center of the specimen. Using the surface strain given by the strain gauges and the formulas in equation 6, the Young's moduli were calculated and displayed in table 38.

Table 38: Experiment 5: Flexural PMMAc testing Surface Young's Moduli

3pb Tensile [GPa]	4pb Tensile [GPa]	4pb Compressive [GPa]
4.1083	4.9726	4.8200

3.2.2 Result Explanation

The specimens marked with "tensile" in table 38 had their strain gauges on the bottom of the sample and in the center, where the maximum deformation was. The specimen marked with "compressive" similarly had its strain gauge in the center, but then at the top, between the two load points of the 4pb test. From table 38 it can be concluded that there is a difference between these two Young's moduli, even though they are of the same specimen. This difference is likely caused by the strain gauge location, as it measures compressive strain on the top and tensile strain on the bottom. Normally the compressive strength and stiffness of PMMA are higher than their tensile counterparts, but this is not shown in the values of table 38. This difference from literature could be due to the strain gauge measuring locally, which means that if it was slightly off from the actual maximum displacement on the bottom, it might have measured less displacement and therefore resulted in a larger stiffness when combined with the maximum stress.
The difference between 3pb tensile and 4pb tensile is also noteworthy. In figure 15 it is clear that the 3-point bending test has a less linear elastic zone than the 4-point bending test with the same specimen and strain gauge location. This is likely due to the tendency of a 3pb test to cause slip on the support pins, which causes the extra strain for less stress. This is shown in the wavy nature of the curve. The average stiffness of this curve will therefore be lower than expected.

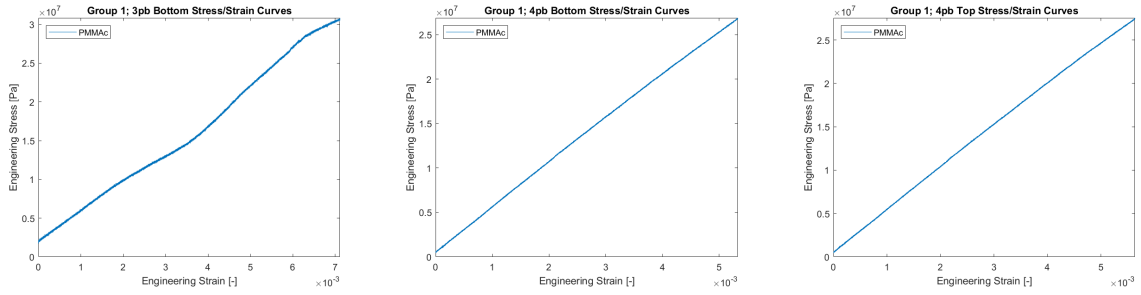

((a)) 3pb Tensile ((b)) 4pb Tensile ((c)) 4pb Compressive

Figure 15: Properties as a function of strain rate

3.2.3 Uncertainty Analysis

For determining the uncertainty of the Young's moduli in table 38, a budget of uncertainties is required. This test used a different displacement measuring technique, which are strain gauges. Due to the changes both these gauges and the new size measurements give, the budget from section 2.1 will be altered for this experiment, which is shown in table 40. As the machine displacement was not used to obtain these parameters, the uncertainties for the grip-to-grip distance will be entirely discarded. The calipers and micrometer are still the same, as is the force transducer. This new gauge factor and transverse sensitivity are found on the cardboard datasheet which came with the strain gauge, and are noted in table 39.

Table 39: Micro-Measurements C2A-06-125LW-120 Strain Gauge Data

Gauge Factor (at 24 $°C$)	Transverse Sensitivity
2.130±0.5%	(+0.8±0.2)%

Table 40: Sources of Uncertainty

Influencing Factor	Error type	Distribution	Error value
1:Width measurement (Calipers: Holex ABS) [2]			
Repeated measurements	A	Gaussian	±0.0058 mm
Resolution	B	Uniform	±0.01 mm
Measurement Deviation E MPE	B	Gaussian	±0.03 mm
2:Thickness Measurement (Micrometer: Mitutoyo IP65) [3]			
Repeated measurements	A	Gaussian	±0.0007 mm
Resolution	B	Uniform	±0.0005 mm
Precision	B	Gaussian	±0.001 mm
3:Strain (Micro-Measurements C2A-06-125LW-120 Strain Gauge) [39]			
Gauge factor	B	Gaussian	0.5 %
Transverse sensitivity	B	Gaussian	0.2 %
4:Force Measuring (KAF-W Force Transducer) [1]			
Accuracy	B	Gaussian	0.05 %
Repeatability	B	Uniform	±2.5 N

As in the previous sections, the combined standard uncertainty of the parameters, in this case the Young's moduli, will be calculated using the type A and B errors using the formulas in equation 1 and 2. These uncertainties are finally displayed in table 41.

Table 41: Experiment 5: Combined standard uncertainties experiment 5: Young's moduli

Specimen	3pb Tensile [GPa]	4pb Tensile [GPa]	4pb Compressive [GPa]
PMMAc	±0.0942	±0.0611	±0.0579

A few assumptions can be made based on these uncertainties. Firstly, the Young's modulus uncertainties are significantly lower than those in section 3.1. This is probably due to the strain gauges, as these have smaller errors in their displacement measurement than the UTM machine displacement has. Also interestingly, the 3-point bending test has about a third higher uncertainty than the 3-point bending tests. This is likely caused by the displacement, as the 3pb test went up yo 2 mm tool displacement, where the 4pb tests only went to 1.5 mm tool displacement, as the maximum displacements for these tests is not equal to the tool displacement. This extra displacement influences the uncertainty for the stress, therefore impacting that of the Young's modulus as well.

4 Conclusion

The experimental campaign provided a comprehensive investigation into the mechanical behavior of metallic and polymeric materials under axial and flexural loading conditions. Through systematic testing and uncertainty analysis, the influence of material composition, manufacturing process, and strain-measurement technique on the derived mechanical properties was thoroughly examined.

For the metallic tensile tests, copper and aluminum specimens exhibited distinct deformation responses consistent with their micro-structural characteristics. Copper displayed pronounced strain hardening and ductile behavior, while aluminum showed a narrower plastic region and a closer proximity between yield and ultimate strengths. The comparison between engineering and true stress–strain analyses confirmed that true parameters are essential for accurate characterization beyond the elastic regime, as they account for cross-sectional reduction during plastic flow. The uncertainty assessment demonstrated that dimensional measurements and load cell precision constitute the primary contributors to experimental variability.

The cyclic strain-measurement experiments revealed clear differences among the extensometer, digital image correlation (DIC), and machine displacement methods. While all three techniques captured the elastic response with reasonable accuracy, the extensometer and DIC methods produced more reliable moduli and yield values due to their direct strain measurement and minimal compliance influence. Inter-group comparison validated these results within the expected experimental tolerance.

The polymeric axial tests emphasized the influence of material type and strain rate on mechanical performance. The ductile response of polypropylene contrasted with the brittle fracture of polystyrene and polymethyl methacrylate (PMMA). Increasing strain rate produced a higher apparent stiffness and strength in PMMA, consistent with viscoelastic rate-dependent behavior. Differences between extruded and cast PMMA further highlighted the impact of manufacturing-induced anisotropy, while local imperfections introduced by laser cutting were identified as potential crack initiation sites.

The flexural tests confirmed that the flexural modulus exceeded the tensile Young's modulus for all polymers, as bending incorporates both tensile and compressive components. The distinction between three- and four-point configurations demonstrated the stabilizing effect of dual load points and the influence of stress concentration under single-point loading. The complementary use of strain gauges in flexural testing enabled precise local strain acquisition, with results confirming predominantly elastic behavior and validating theoretical assumptions on beam bending.

Overall, the combination of axial and flexural experiments established a coherent understanding of elastic, plastic, and failure mechanisms across different materials and loading conditions. The consistent treatment of measurement uncertainties strengthened the reliability of the derived parameters. The findings underscore the critical role of strain-measurement technique, strain rate, and specimen geometry in the accurate experimental characterization of materials within the field of experimental mechanics.

References

[1] "AST". "product information: Kaf w force transducer". URL "https://www.ast.de/en/products/force-measurement-technology-sensor-systems/sensors/kaf-w".

[2] "Holex". "digital caliper abs with rod type depth gauge, measuring range: 150mm". URL "https://www.hoffmann-group.com/US/en/hus/p/412818-150".

[3] "Mitutoyo". "digitale micrometer 0-25 mm ip65". URL "https://www.manutan.nl/nl/mnl/digitale-micrometer-0-25

[4] Tusit Weerasooriya Wayne Chen" "Paul Moy, C. Allan Gunnarsson. "stress-strain response of pmma as a function of strain-rate and temperature". URL "https://www.researchgate.net/publication/227264277$_{S}tress - Strain_{R}esponse_{o}f_{P}MMA_{a}s_{a}_{F}unction_{o}f_{S}train - Rate_{a}nd_{T}emperature$".

[5] "Zwick Roell". "product information: Xforce k load cells", . URL "https://www.zwickroell.com/fileadmin/content/Files/SharePoint/user$_{u}pload/PI_{E}N/03_{6}77_{X}force_{K}load_{c}ells_{I}$

[6] "Zwick Roell". "product information: Materials testing machines proline z005 to z100", . URL "https://www.zwickroell.com/fileadmin/content/Files/SharePoint/user$_{u}pload/PI_{E}N/02_{3}75_{P}roLine_{Z}005_{u}p_{t}o_{Z}$

[7] "Zwick Roell". "product information: Clip-on extensometer 5025-1, 8040-1 and 7537-1", . URL "https://www.zwickroell.com/fileadmin/content/Files/SharePoint/user$_{u}pload/PI_{E}N/08_{9}25_{C}lip_{o}n_{e}xtensomet$

[8] "Zwick Roell". "product information: zwickiline materials testing machines z5.0", . URL "https://senselektro.hu/wp-content/uploads/zwick/zwicki-Line-Fmax-5-kN1.pdf".

[9] "Mississipi State University". "section ii.4 inelastic bending of homogeneous beams". URL "https://www.ae.msstate.edu/tupas/SA2/chA13.10$_{t}ext.html$".

[10] "welleshaft". "flexure vs. young's modulus: Definitions and formulas". URL "https://welleshaft.com/es$_{p}e/flexural - modulus - vs - youngs - modulus - vs - elastic - modulus/ : : text = The\%20Main\%20Difference : \%20The\%20Type, for\%20the\%20same\%20practical\%20measurement.$".